ACS OMEGA

http://pubs.acs.org/journal/acsodf

Article

Condensation Separation of NO_2 with Dimerization Reaction in the Presence of Noncondensable Gas: Critical Assessment and Model Development

Yingshu Liu, Jiaxin Liu, Ziyi Li,* Ningqi Sun, Xiong Yang, Huanyu Hou, Wenhai Liu, Chunyu Zhao, and Ralph T. Yang

Cite This: *ACS Omega* 2022, 7, 14735−14745

Read Online

ACCESS | Metrics & More | Article Recommendations | Supporting Information

ABSTRACT: Pure nitrogen dioxide (NO_2) has significant economic value and is widely used in many fields, for which condensation technology plays an important role in separation and purification. However, developing cost-effective NO_2 condensers remains challenging due to the lack of precise theoretical guidelines and comprehensive understanding of NO_2 condensation process. In this work, NO_2 condensation at various inlet surface subcoolings, mole fractions of noncondensable gas (NCG), and *Re* numbers was studied with a visualization experimental system. The influential rules of each parameter on heat transfer coefficients (HTCs) and the NO_2 condensate state as the coexistence of droplet, streamlet and film were revealed. A substantial underestimation of experimental data by the classical heat and mass transfer analogy (HMTA) model was quantified. The large discrepancy was found to originate from the uniqueness in heat transfer, mass transfer, and condensate state caused by NO_2 dimerization during condensation. A modified HMTA model was developed considering the release heat of dimerization reaction and the promotion of mass transfer by an increased NO_2 concentration gradient within the diffusion layer which contribute to improvements of HTCs by ∼6 and ∼49%, respectively. The correction of liquid film roughness regarding potential heterogeneity of dimerization was proposed as a function of the key parameters, contributing to the improvement of HTCs by ∼150%. An accurate theoretical formula for HTCs prediction within an error of ±25% was finally derived, providing the key step for success in practical applications.

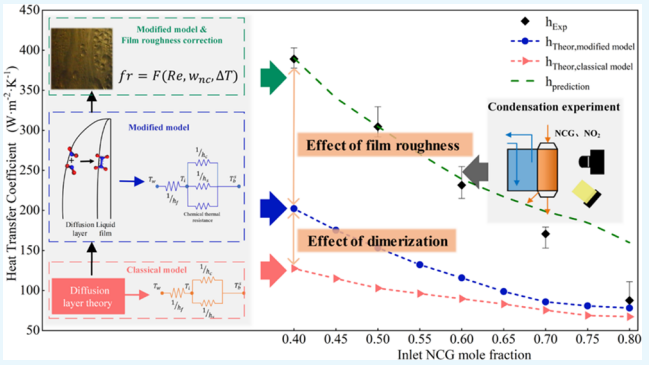

1. INTRODUCTION

Nitrogen dioxide (NO_2) is a valuable chemical in many fields, which has extensively been used as a multifunctional reagent (nitration agent, nitrosation agent and oxidant), a rocket propellant[1,2] and important ingredients of nitric acid and dimethyl sulfoxide. The high-purity NO_2 liquid product has a market price of ∼6000 U.S. dollars/ton in China. The ways of acquiring high-purity NO_2 involve separating NO_2 from products of ammonia catalytic oxidation as the conventional production process[3] and recycling NO_2 from rocket-launching exhaust gases[4] and industrial flue gases.[5,6]

NO_2 with a standard boiling point of 294 K can be upgraded and liquefied with high purity and recovery under mild operation conditions, based on which the condensation technology plays an important role in NO_2 separation, purification, and storage in each NO_2 acquisition process. Zhang et al.[7] demonstrated the condensation process of recycling NO_2 from the rocket-launching exhaust gas, achieving a NO_2 purity of 99.6% and a recovery of 95.6% under the conditions of 0.12 MPa and 263.15 K. Liu et al.[8] proposed a condensation−distillation process capable of recycling NO_2 from iron-ore sintering flue gas and obtained high-purity (>99.5%) NO_2 liquid at 0.1 MPa and 263.95 K. Although the NO_2 condensation technology has been applied in industry, there remain significant problems such as high investment, operation cost, and safety hazards due to the bulky condenser, equipment corrosion, and high condensation pressure, respectively. Therefore, it is a long-sought-after goal to improve the energy efficiency of NO_2 condensation to reduce the size of the condenser and the operation complexity. To meet this goal, precise theoretical guidance is necessary[9,10] for condenser design and optimization, for which effects of processing parameters on NO_2 heat and mass transfer during the condensation merit investigations from the following three

Received: January 2, 2022
Accepted: April 7, 2022
Published: April 21, 2022

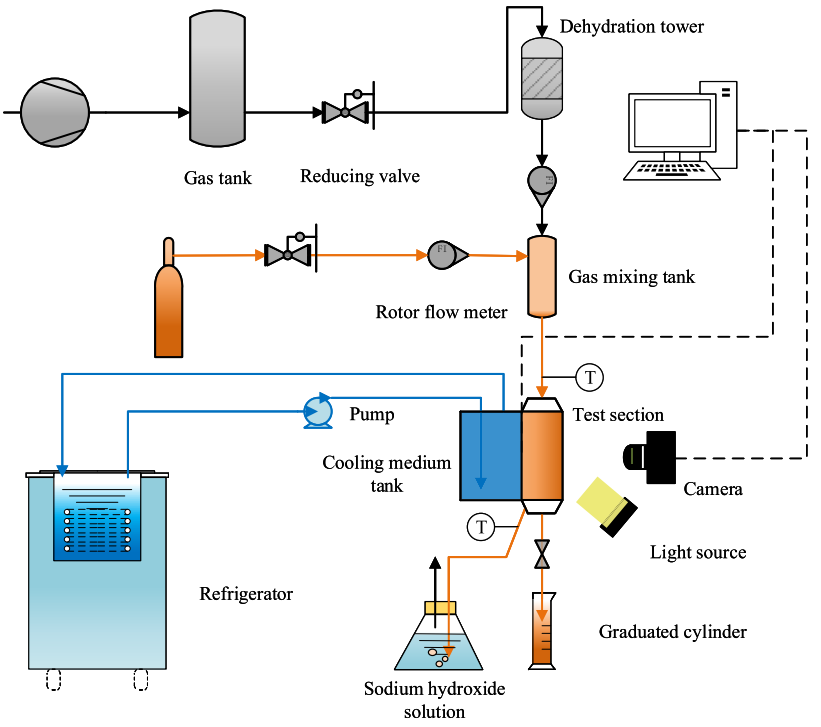

(a)

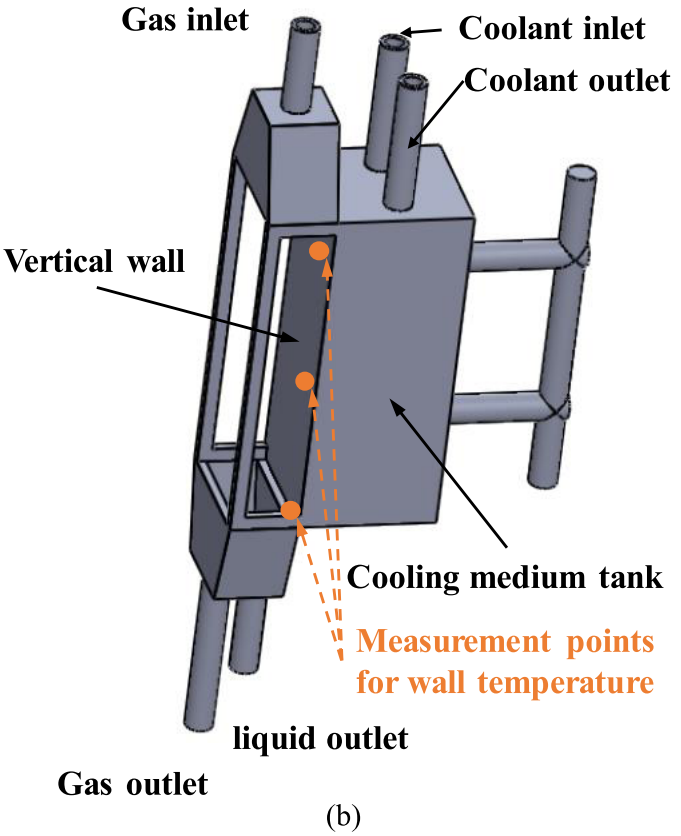

(b)

Figure 1. Schematics of (a) condensation experimental system and (b) test section.

perspectives. First, coexisting noncondensable gases (NCG including N_2, O_2, etc.) impair NO_2 condensation efficiency, for which studies on water vapor condensation have shown that a 0.5% volume fraction of air can reduce the heat transfer coefficient (HTC) by 50%.[11,12] Second, the conversion of NO_2 to N_2O_4 is favored at lower temperatures via the exothermic

https://doi.org/10.1021/acsomega.2c00013
ACS Omega 2022, 7, 14735−14745

dimerization reaction, which may lead to changes in the NO_2 gaseous concentration and bulk gas temperature.[13,14] Third, the effect of the condensate film roughness on heat and mass transfer within the diffusion layer (gaseous region between the bulk and the film)[15,16] could not be ignored,[17,18] particularly as the NO_2 dimerization is involved.

Previous studies on gas condensation in the presence of NCG and the effects of liquid film roughness were mainly focused on water vapor. In terms of the effect of NCG, Peterson et al.[15] developed a diffusion layer model and accurately predicted the experimental condensation Nusselt (Nu) number in the presence of NCG with a minimum standard deviation of 4.7%. Dehbi et al.[19] developed a heat and mass transfer analogy (HMTA) model, showing that the increase of NCG from 5 to 10% suppressed heat transfer in water vapor condensation (inlet Nu from 500 to 425). Ge et al.[20] experimentally studied the effects of NCG (CO_2) at a wide concentration range on water vapor condensation, showing that the increase of the CO_2 mass fraction from 23.3 to 84.0% resulted in the decrease of HTC from 5.5 to 1 $kW{\cdot}m^{-2}{\cdot}K^{-1}$. In terms of the effect of film roughness, a degradation factor defined as the ratio of experimental HTC to theoretical HTC has been commonly employed to correct the error caused by interfacial shear stress while using the conventional models. Lee and Kim[21] showed a satisfactory prediction accuracy with a standard deviation of 19.5−25.8%, by correcting the laminar film model with the degradation factor. Kuhn et al.[22] improved Nusselt film model prediction with the relative standard deviation of 17.6% for HTC by adopting a degradation factor and addressed the heat transfer enhancement due to interfacial shear and surface waviness. Ren et al.[23] used the HMTA model in consideration of film roughness and found that the increase of the inlet mixture mass flux (from 55 to 165 $kg{\cdot}m^{-2}{\cdot}s^{-1}$) increased the heat flux by 110%, indicating the positive effect of film roughness on heat transfer. In terms of gas vapor condensation in consideration of dimerization reaction, Gribkova[13] found that the prediction quantity of condensed N_2O_4 with the model considering the dimerization reaction was 1.24−1.12 times higher than that without dimerization. Mikhalevich[14] found that NO_2 dimerization chemical reactions promoted gas saturation temperature and the heat transfer rate. To sum up, the combined effects of NCG, liquid film roughness, and dimerization reaction on NO_2 condensation were rarely studied, which may largely be associated with the difficulties in measuring NO_2 condensation variables regarding the narrow condensation temperature range (from a freezing point of 262.15 K to a boiling point of 294.15 K) and the highly corrosive experiments.

In this study, a NO_2 condensation experiment apparatus coupled with a sophisticated methodology was set up. The HMTA model in consideration of NO_2 dimerization was developed. With the aim of guiding practical application, NO_2 condensation at various surface subcoolings, NCG mole fractions, and the inlet mixture Reynolds number (Re) was systematically investigated through a series of condensation tests. The influential rules of each processing parameter on HTCs and the coexistence of droplet, streamlet, and film as the stabilized NO_2 condensate state were revealed. The key roles of the NO_2 dimerization reaction and the film roughness in condensation were revealed and explored by comparing experimental data and model-predicted results. The friction factor (f_r) correlated with the condensate flow rate as a function of Re, inlet surface subcooling, and NCG mole fraction was proposed to gain deeper insights into NO_2 condensation and improve the model prediction accuracy for practical use.

2. EXPERIMENTAL METHOD

2.1. Experimental System. The NO_2−air condensation experimental system consisted of a gas supply system, a gas flow rate control system, a refrigerant circulation system, a data acquisition system, and a test section, as shown in Figure 1a. In current work, the gas supply system used only air as NCG, which is close to the real situation that the concentrations of other NCGs such as NO are much lower as compared with air. The inlet air provided by the air compressor passed through the reducing valve capable of stabilizing the pressure and then entered the dehydration column. The NO_2 (purity > 99.9%) was supplied by the gas cylinder, whose pressure was controlled by a reducing valve at the outlet of the tank. The gas flow rates of air and NO_2 were controlled by rotameters. The two gases were fully mixed in the mixing tank where a constant temperature of 303.15 K was achieved by heating tape to prevent NO_2 condensation. The gas mixture was then fed into the test section for condensation, and the NO_2 condensate can be collected using a measuring cylinder.

The test section made from 316 stainless steel was the core part of the experimental system. The structure of the test section is shown in Figure 1b, with detailed information listed in Table 1. Three T-type patch thermocouples were set for measuring the wall temperature. Another three T-type thermocouples for measuring the bulk mixture temperature were set above the corresponding wall temperature measuring point. In addition, two T-type thermocouples were set in the gas inlet and outlet pipes to measure the temperature of the mixture gas. All thermocouples were connected to an Agilent data collector. Transparent glass sheets were glued around the wall to ensure that the device was sealed. Two high-definition cameras were placed on the front and side of the test section to photograph the condensate. Through this kind of visual design, it was able to ensure that there was no frozen NO_2 during the experiment and the data can be measured accurately. A medium tank filled with a coolant was connected directly behind the wall and was covered with insulation material to prevent energy loss. The coolant driven by a centrifugal pump consisted of ethylene glycol and water, circulating between the cooling medium tank and the refrigerator, and providing cold energy to the test section.

Table 1. Detailed information of the Test Section

items	details
length of the rectangular channel	0.030 m
width of the rectangular channel	0.015 m
length of the vertical wall	0.075 m
width of the vertical wall	0.030 m
thickness of the vertical wall	0.0008 m
distance between thermocouples on the wall	0.025 m
distance between the bulk mixture temperature measuring point and the wall	0.0075 m

2.2. Data Reduction. According to the law of conservation of energy, the total heat flow rate between the bulk mixture and the wall originating from the sensible heat $\dot{Q}_s$, the latent heat $\dot{Q}_{cd}$, and the chemical heat $\dot{Q}_r$ from a potential dimerization reaction can be expressed as

https://doi.org/10.1021/acsomega.2c00013
ACS Omega 2022, 7, 14735−14745

$$\dot{Q} = \dot{Q}_s + \dot{Q}_{cd} + \dot{Q}_r = C_p q_m (T_{in} - T_{out}) + h_{fg}\rho_{NO_2,l} V_{NO_2,l}/t + \dot{Q}_r \quad (1)$$

where $\dot{Q}_s$ was calculated by the temperature measured from the inlet and outlet pipes and $\dot{Q}_{cd}$ was calculated by the amount of the condensate and the corresponding time difference in a steady state. The calculation method of $\dot{Q}_r$ was as follows. According to the chemical equation of NO_2 and N_2O_4, the reaction constant[24] can be determined from

$$K_p = p_{NO_2}{}^2/p_{N_2O_4} \quad (2)$$

where p_{NO_2} and $p_{N_2O_4}$ are the partial pressures of NO_2 and N_2O_4, respectively. The relationship between the mole fraction of NO_2 and K_p at reaction equilibrium is written as

$$K_p = (w_{NO_2}P)^2/(1 - w_{NO_2})P \quad (3)$$

$$w_{NO_2} = 0.5(-K_p/P \times (1-\sqrt{1 + 4P/K_p})) \quad (4)$$

As shown in eq 4, only K_p of the reaction is required for calculating the mole fraction of NO_2 at a constant total pressure P. Chao et al.[25] concluded the correlation between K_p and temperature as

$$\log_{10} K_p = -4.704 + 6.9628 \times 10^{-4}T - 2691.09/T + 9.981163 \log_{10} T - 14.284 (1 + 85/T) \log_{10} (1 + T/85) - 6.6794 \times 10^{-8}T^2 \quad (5)$$

According to the relation of chemical reaction coefficients (as described in the Section S3 of the Supporting Information), the chemical heat flow rate from the initial state (with pure NO_2) to the equilibrium of the reaction is

$$\varphi[w_{NO_2}(P, T), q_{mNO_2}] = 57 \times 10^3 \times (1 - w_{NO_2})q_{mNO_2}/[(2 - w_{NO_2})M_{NO_2}] \quad (6)$$

The reaction heat from equilibrium state A to equilibrium state B can be calculated by the difference between the heat released from the initial state to two states. Figure 2 shows the material flow and energy flow of NO_2 above the wall. Thinking of the test section as one node in Figure 2, the dimerization process in the condenser can be classified into dimerization of gaseous NO_2 that is not condensed flowing from the inlet to the outlet and the dimerization of gaseous NO_2 that would be condensed from the bulk gas to the wall.

The mass flow rate of NO_2 involved in both dimerization processes can, respectively, be expressed as

$$q_{mNO_2,1} = q_{mNO_2,out} \quad (7)$$

$$q_{mNO_2,2} = \rho_{NO_2,l} V_{NO_2,l}/t \quad (8)$$

where $q_{mNO_2,out}$ is the mass flow rate of NO_2 at the gas outlet pipe. $\rho_{NO_2,l}$ is the density of liquid NO_2, $V_{NO_2,l}$ is the volume of liquid NO_2 collected in a steady state, and t is the collection time. The inlet and outlet temperatures were selected as the NO_2 saturation temperatures of the equilibrium states at the inlet and the outlet. The average temperatures of the wall and the bulk mixture (eqs 9 and 10) were selected as the NO_2 saturation temperatures of the equilibrium states at centroid points of the wall and the gas flow channel, respectively.

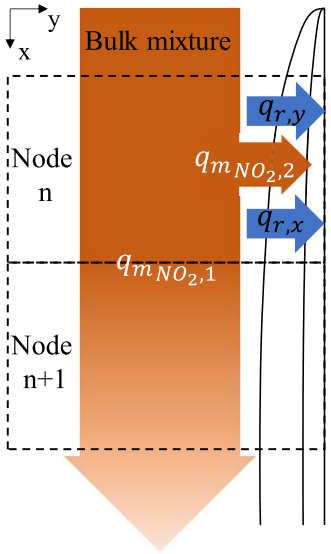

Figure 2. Material flow and energy flow of condensation with the dimerization reaction.

$$\overline{T_W} = \frac{1}{3}\sum_{i=1}^{3} T_{W,i} \quad (9)$$

$$\overline{T_b} = \frac{1}{3}\sum_{i=1}^{3} T_{b,i} \quad (10)$$

Based on eq 6, the chemical heat flow rate is expressed as

$$\dot{Q}_r = \dot{Q}_{r,y} + \dot{Q}_{r,x} = \varphi(w_{NO_2}(P, T_{out}), q_{mNO_2,1}) - \varphi(w_{NO_2}(P, T_{in}), q_{mNO_2,1}) + \varphi(w_{NO_2}(P, \overline{T_W}), q_{mNO_2,2}) - \varphi(w_{NO_2}(P, \overline{T_b}), q_{mNO_2,2}) \quad (11)$$

The average HTC of the test section is calculated from

$$h = \dot{Q}/A(\overline{T_b} - \overline{T_W}) \quad (12)$$

3. THEORETICAL MODEL

Classical and modified HMTA condensation models were built in this work. The classical model referred to the conventional diffusion layer model[16,19,21,23] in predicting water vapor condensation, where the total HTC consists of liquid film HTC, sensible HTC, and latent HTC, in terms of the effects of NCG on condensation. The modified model was developed considering the dimerization of NO_2 in the diffusion layer on the basis of the classical model. Similar to the correction of enhanced heat transfer due to film roughness in previous studies,[21,22] a degradation factor was introduced to correct the underestimation of experimental HTC. Through the comparisons of two models with experimental data, the effects of dimerization reaction and the film roughness on heat and mass transfer would be demonstrated, for the purpose of accurate

https://doi.org/10.1021/acsomega.2c00013
ACS Omega 2022, 7, 14735−14745

prediction of practical NO_2 condensation. The detailed derivations for the models were described as follows.

3.1. Classical HMTA Model. The classical HMTA model, based on the diffusion layer theory,[15] suggests that condensable gas condenses to form a liquid film with the thickness of δ, and NCG that cannot pass through the film but only accumulates on the film surface forms a stable diffusion layer of mixed gas outside the liquid film. According to the conservation of energy, the heat transfer through the gas diffusion layer is equal to that through the condensate film. Therefore, both the latent heat (the heat flux is q_{cd}) of the condensed vapor and the sensible heat (the heat flux is q_s) of the mixed gas first pass through the diffusion layer and then through the film. The equivalent thermal resistance diagram is shown in Figure 3a.

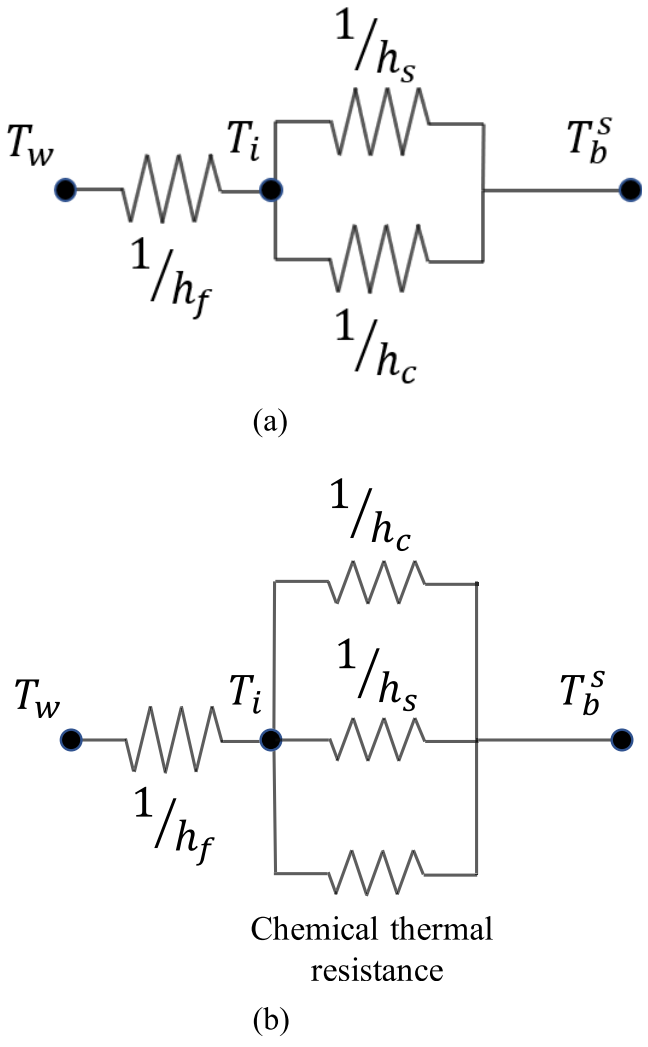

Figure 3. Equivalent thermal resistance diagrams of (a) classical HMTA model and (b) modified HMTA model.

The heat balance can be expressed as

$$q = q_{cd} + q_s = m''_{NO_2} h_{fg} + h_s(T_b^s - T_i) = h_f(T_i - T_w) \tag{13}$$

where h_f is the liquid film HTC and h_s is the sensible HTC. The latent HTC can be defined as

$$h_c = m''_{NO_2} h_{fg}/(T_b^s - T_i) \tag{14}$$

The total HTC can be defined as

$$h = q/(T_b^s - T_w) \tag{15}$$

Since the temperatures in eq 15 are the initial values, to calculate the total HTC, the interface temperature should be assumed at first and then calculated h_f, h_c, and h_s. Finally, the steady-state values of all parameters are iteratively calculated.

The suggestion of Nusselt is adopted for h_f, and is given by

$$h_f = \lambda_l/\delta = \left[\frac{\rho_l(\rho_l - \rho_i)g h_{fg} \lambda_l^3}{4\mu_l(T_i - T_w)x}\right]^{0.25} \tag{16}$$

The theory of diffusion layer is adopted for h_c (Sections S4 and S5 of the Supporting Information show more details), and is calculated by

$$h_c = Sh\frac{\rho_{mix} D h_{fg}}{(T_b^s - T_i)L}\ln\left(\frac{w_{m,air_i}}{w_{m,air_b}}\right) \tag{17}$$

The total length of the test section is too short (0.075 m) to allow the gas to reach the fully developed stage. The Haji-Sheikh's[26] correlation of forced convection at the entrance of vertical plate is adopted to calculate Sh

$$Sh_L = \frac{3.106}{\hat{x}^{1/3}} + \frac{7.541}{[1 + 112\hat{x}^{-0.9}/125]^{3/4}} \tag{18}$$

where $\hat{x} = (x/a)/Pe$, a is half of the flow channel thickness and a = 0.0075 m in this model. Pe is the Peclet number, which is defined as $Pe = ReSc$ for mass transfer.

The h_s in the diffusion layer is also calculated by Haji-Sheikh's correlation

$$Nu_L = \frac{h_s L}{\lambda} = \frac{3.106}{\hat{x}^{1/3}} + \frac{7.541}{[1 + 112\hat{x}^{-0.9}/125]^{3/4}} \tag{19}$$

For the heat transfer process, Pe is defined as $Pe = RePr$.

The suction effect can thin the diffusion layer of the mixed gas, leading to enhancement of the heat and mass transfer.[27] A correction factor has been introduced to correct the enhancement caused by the suction effect

$$Sh' = \frac{\ln(1 + B_m)}{B_m} Sh \tag{20}$$

$$Nu' = \frac{\ln(1 + B_h)}{B_h} Nu \tag{21}$$

where mass transfer blowing parameter B_m and heat transfer blowing parameter B_h are defined as

$$B_m = \frac{w_{NO_2,i} - w_{NO_2,b}}{1 - w_{NO_2,i}} \tag{22}$$

$$B_h = \frac{m''_{NO_2} C_{p,NO_2}}{h_c} \tag{23}$$

3.2. Modified HMTA Model. The modified HMTA model was modified from two aspects of chemical heat and the change of physical properties. During the diffusion of NO_2 toward the lower temperature film surface, two NO_2 molecules dimerize to form one N_2O_4, releasing reaction heat energy and reducing the concentration of condensable components in the diffusion layer. Based on the above process, the modified HMTA model is established as follows.

https://doi.org/10.1021/acsomega.2c00013
ACS Omega 2022, 7, 14735−14745

The total heat flux is composed of q_{cd}, q_s, and the chemical heat flux q_r. Based on the sketch of the modeled systems shown in Figure 2, the equivalent thermal resistance diagram of the modified model is shown in Figure 3b. The heat balance between the diffusion layer and the film is expressed as

$$q = q_r + q_{cd} + q_s = q_r + m''_{NO_2} h_{fg} + h_s(T_b^s - T_i) = h_f(T_i - T_w) \quad (24)$$

The modification method of chemical heat in the model is similar to that in Section 2.2. A one-dimensional mesh is built for the vertical wall along the direction of gas flow, as shown in Figure 2. The dimerization reaction is assumed in two directions: direction 1 corresponding to condensed NO_2 and N_2O_4 is perpendicular to the wall, and direction 2 corresponding to uncondensed NO_2 and N_2O_4 is parallel to the wall. The temperature of the gas−liquid interface approximately equals the wall temperature, thus we ignore the reaction in the liquid film and consider that the reaction of direction 1 mainly occurs in the diffusion layer. Accordingly, the dimerization in direction 1 is caused by the temperature difference between the bulk gas and the interface, releasing heat flux $q_{r,y}$. The dimerization reaction in direction 2 is caused by the gas temperature difference between node n and node n+1, releasing heat flux $q_{r,x}$. The $q_{r,y}$ and $q_{r,x}$ can be calculated from

$$q_{r,y} = \varphi_n(w_{NO_{2_i}}, m''_{NO_2}) - \varphi_n(w_{NO_{2_b}}, m''_{NO_2}) \quad (25)$$

$$q_{r,x} = [\varphi_{n+1}(w_{NO_{2_b}}, q_{mNO_2,n+1}) - \varphi_n(w_{NO_{2_b}}, q_{mNO_2,n+1})]/A \quad (26)$$

Both parts of the heat exchange caused by the dimerization reaction occur at the current node, so the total reaction heat flux of the node n is the sum of the two

$$q_r = q_{r,x} + q_{r,y} \quad (27)$$

At the steady state of test section's temperature field and dimerization, parameters of all gases can be calculated from temperature, pressure, and mole fraction. The total HTC of the node can be calculated by eqs 15,24 and 27.

3.3. Film Roughness Correction. In conventional investigations on water condensation, the uneven condensate surface can inevitably be formed due to the wavy surface caused by a turbulent flow regime, resulting in the film roughness that depends on Re, and needs to be considered into the theoretical model for accurate prediction. For the NO_2 condensation in this work, the film roughness for the NO_2 condensate may also exist even at a laminar flow, as will be shown in Section 4.3, due to the potential inhomogeneity of condensation in terms of the specialty of NO_2 dimerization exothermic process that highly depends on temperature (ΔT) and the NCG mole fraction (w_{nc}). Therefore, the correlation of film roughness ought to be conducted.

The classical film roughness correction method for water vapor condensation is as follows[23]

$$Sh'' = Sh' f_c \quad (28)$$

$$Nu'' = Nu' f_c \quad (29)$$

The correction for the film roughness f_c is given as

$$f_c = (f_r/f_s)^n \quad (30)$$

where $f_s = 16.2/Re$, $n = Pr^{0.36}$ for correcting Nu', and $n = Sc^{0.36}$ for correcting Sh'.

The friction factor f_r is a degradation factor, the ratio of experimental HTC to the original predicted HTC, which can be used to improve the accuracy of water−NCG condensation model prediction.[21,22] The f_r for film roughness of water is as follows

$$f_r = 1.375 \times 10^{-3}[1 + 21.544 \times (100/Re)^{1/3}] \quad (31)$$

Although the classical friction factor f_r without consideration of dimerization may not be applicable to NO_2 condensation, the relationships between the variables above can be adopted to get degradation factor f_r for NO_2. In this work, f_r is assumed to be related not only to Re, indicative of fluid mechanical properties, but also to ΔT and w_{nc}, indicative of NO_2 dimerization properties. The friction factor follows the function as $f_r = f(Re, w_{nc}, \Delta T)$, and the detailed relationships among the parameters are derived and validated in Section 4.3.

4. RESULTS AND DISCUSSION

4.1. Effects of Various Parameters on Average HTC. *4.1.1. Effects of Surface Subcooling on HTC.* Figure 4 shows

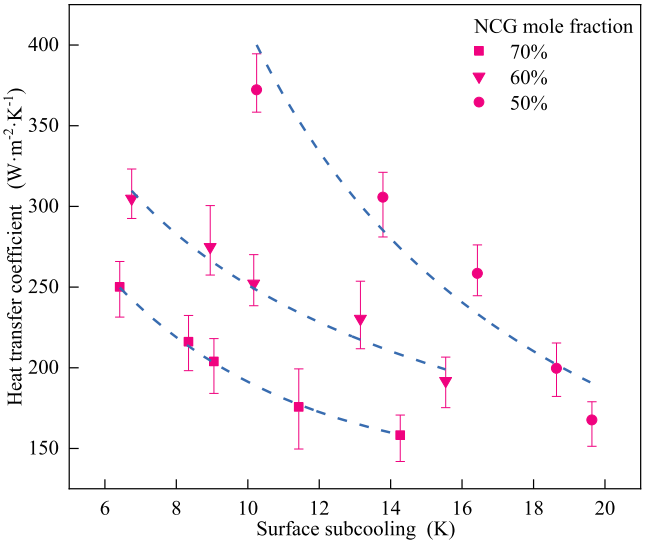

Figure 4. Effect of surface subcooling on the average HTC.

the dependence of average HTC on surface subcooling at a 500 mL·min^{-1} inlet mixture volume flow and NCG concentrations of 50, 60, and 70%, respectively. In the range of surface subcooling (6−20 K), the average HTC decreases with increasing surface subcooling. For the lower NCG mole fraction, the decreasing trend is sharper: an increase in the surface subcooling by 20 K causes HTC to drop by about 200 W·m^{-2}·K^{-1}.

According to Figure 3b, total HTC is composed of h_f, h_c, and h_s and the equivalent HTC of chemical heat. Generally, h_f and h_c involving latent heat as the major contribution to total heat transfer dominate the value of HTC.[16] For h_f, the increase in surface subcooling promotes NO_2 condensation and thus increases the thickness of the liquid film, leading to the decrease of h_f. For h_c, the main thermal resistance that deteriorates the condensation heat transfer is in the diffusion layer.[20] The higher NO_2 condensation rate with the increased surface subcooling promotes the accumulation of NCG at the gas−liquid interface,

https://doi.org/10.1021/acsomega.2c00013
ACS Omega 2022, 7, 14735−14745

thus increasing the mass transfer resistance according to the diffusion layer theory,[15] and resulting in the decrease of h_c. The sharper decreasing trend of HTC versus surface subcooling at a lower NCG mole fraction is associated with more significant inhibition of heat and mass transfer caused by a greater increase in the NCG accumulation.

4.1.2. Effect of the NCG Concentration on HTC. Figure 5 shows the effects of the NCG mole fraction on average HTC

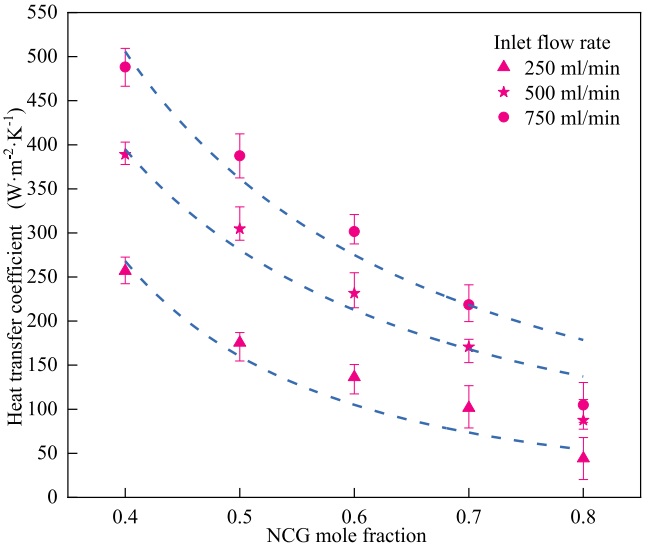

Figure 5. Effect of the NCG mole fraction on the average HTC.

when the surface subcooling is 13 K, and the inlet flow rates of the mixture are 250, 500, and 700 mL·min^{-1}, respectively. The average HTC decreased exponentially with the inlet NCG mole fraction, and there are no significant differences in decreasing trends under different flow rates.

The negative effect of NCG on NO_2 condensation heat transfer can be explained as follows. With the continuous condensation of NO_2, the air gathered on the film surface and formed the diffusion layer.[28,29] Vapor molecules can only reach the film surface by diffusion. The increase in the inlet air mole fraction increases the concentration of NCG in the diffusion layer, suppressing the mass transfer process. Moreover, NO_2 saturation temperature decreases with increasing NCG partial pressure, which also has a negative effect on condensation.

4.1.3. Effect of Re on HTC. Figure 6 shows the variation of HTC with inlet *Re* at a constant pressure when the concentration of NCG is 40, 50, and 60%, respectively. It can be seen from the figure that the HTC increases with inlet *Re*, and the dependence of HTC on *Re* is almost linear in the entire range.

The positive effect of *Re* on NO_2 condensation heat transfer can be explained as follows. With other parameters constant, the increase of *Re* accompanied by the increase of the inlet volume flow rate means that more condensable gas (NO_2 and/or N_2O_4) flows into the test section. With a sufficient supply of cold energy, the heat released from the phase change of the condensable gas increases the heat transfer flow rate and HTC. In terms of the heat and mass transfer, h_c and h_f are the major contributors to HTC and both increase with *Re*. In the aspect of h_c, the increase of *Re* reduces the thickness of the boundary layer and promotes the diffusion rate of NO_2 toward the liquid film. In the aspect of h_f, the increase of *Re* results in a more significant shear force between the gas and the film and

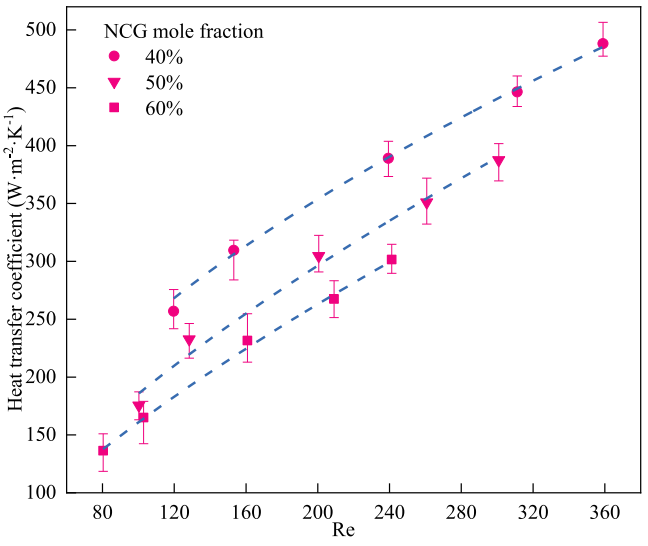

Figure 6. Effect of Re on the average HTC.

perturbs the liquid film,[18,30] making the film thin and reducing the heat transfer resistance of the liquid film.

4.2. Effect of Dimerization on Heat Transfer. Figure 7a,b compares the results of HTC varying with the NCG mole fraction and *Re* from experiments, model predictions from classical and modified HMTA models. As can be seen from the figures, the HTC resulted from the modified HMTA model is closer to the experimental data as compared to that from the classical model. These results indicate the positive effect of NO_2 dimerization on heat transfer. As shown in Figure 7a, with the increase in the NCG mole fraction from 0.4 to 0.8, the HTC calculated by the modified HMTA model is decreased by 61.4%, from 202.2 to 78.0 W·m^{-2}·K^{-1}, whereas the HTC calculated by the classical model is decreased by 47.3%. Obviously, the influence of NCG is more distinct in the former case, and the difference in calculated HTCs between two models (ΔHTC) decreases exponentially with the inlet NCG mole fraction. The reason for this trend could be explained by the fact that the increase in the inlet NCG mole fraction causes less NO_2/N_2O_4 flow over the wall, leading to the decrease in NO_2 molecules involved in the dimerization. However, the proportion of NO_2 in condensable components increases exponentially with the decrease of the partial pressure of the condensable NO_2/N_2O_4 mixture (as described in Section S6 of the Supporting Information). This mechanism can to some extent impede the decrease of dimerization caused by the increase of NCG.

As shown in Figure 7b, with the increase of *Re* from 100 to 300, the HTCs from the modified HMTA model increase at a higher rate (by up to 160.4%) as compared with those from the classical model (127.9%). Meanwhile, the ΔHTC shows an increasing trend with the increase of *Re*. This might be associated with the reduced temperature of the thinned boundary layer at increased *Re*.[31] The lower temperature facilitates the NO_2 dimerization that further promotes the heat transfer.

Figure 8 shows the contributors (latent heat, sensible heat, chemical heat) to the NO_2 condensation heat flow rate predicted by the modified model, and the HTCs predicted by modified and classical models and their differences (ΔHTC) at varying inlet flow rates. Under the inlet surface subcooling of 20 K and the NCG mole fraction of 50%, the total heat flow rate increases from 6.41 to 9.32 J·s^{-1}, as the inlet flow rate increases

https://doi.org/10.1021/acsomega.2c00013
ACS Omega 2022, 7, 14735−14745

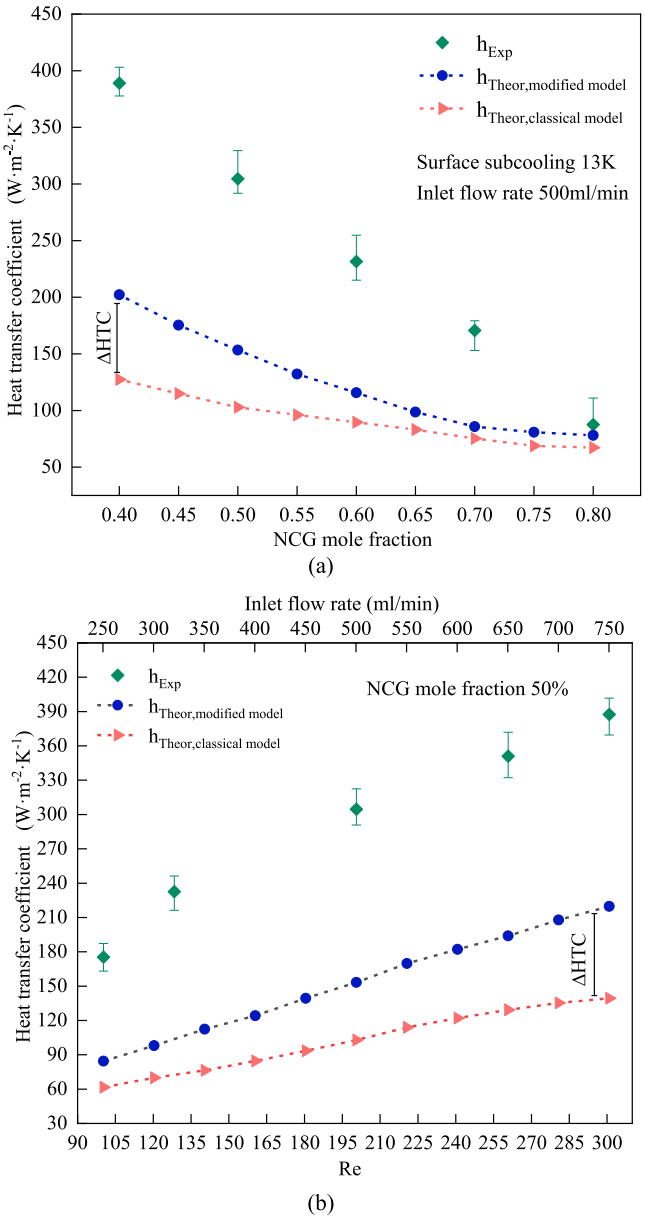

Figure 7. Variation of experimental and theoretical HTCs with (a) NCG mole fraction and (b) *Re*.

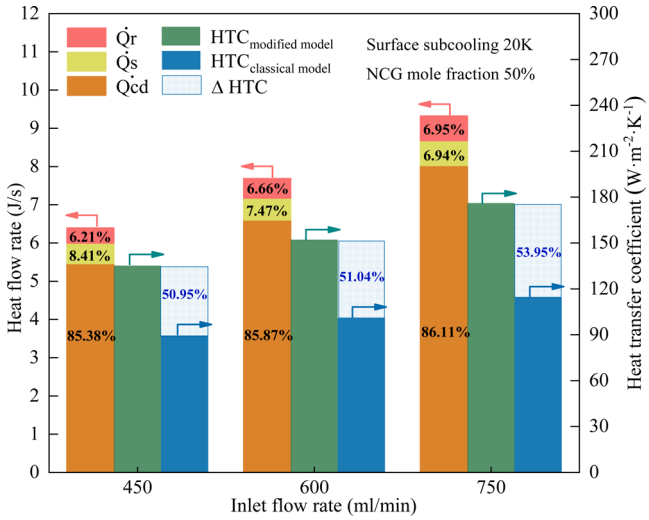

Figure 8. Effect of dimerization on the heat flow rate and HTC.

from 450 to 750 mL·min^{-1}. The latent heat of condensation is found to be the majority (~86%) of the total heat flow, while the dimerization chemical heat and the sensible heat merely account for ~6 and ~8%, respectively. In contrast to the slight effect of dimerization on the heat flow rate, HTC was greatly influenced by dimerization, as evidenced by the relative increase in HTC from the classical model prediction to the modified counterpart ($\Delta HTC/HTC_{classical\ model}$ = 50.95−53.95%).

It can be clearly found that the relative increase in HTC due to dimerization is much greater than that in the dimerization chemical reaction heat, indicating underlying influences of NO_2 dimerization on condensation heat transfer as compared to the direct influence caused by the reaction heat. Considering the process that NO_2 molecules diffuse to the wall and dimerize to N_2O_4, the first underlying influence of NO_2 dimerization might be associated with more gaseous NO_2 driven to the film by a greater concentration gradient of NO_2 between the bulk mixture and the interface due to a reduced number of NO_2 molecules at the interface. As a result, NO_2 condensation and the release of latent and chemical heat would be promoted. In addition, the reduction in NO_2 partial pressure leads to a decrease in the temperature of the bulk mixture, which is assumed to be equal to the saturation temperature of gaseous NO_2. According to Newton's cooling law (eq 15), an increased heat flow and a reduced temperature difference between the bulk and the surface synergistically increase HTC. Note that the average surface subcooling was different at different inlet flow rates though the inlet surface subcooling was kept constant. As a result, the increase in HTC is much greater than the increase in the total heat flow, as shown in Figure 8.

It can be inferred that the influence of dimerization on condensation ought to involve several aspects. In addition to the above heat release or mass transfer effect, the dimerization would also cause other indirect effects from the perspective of a fluid mechanism, as indicated by the remarkable discrepancy between experimental and modified HMTA model results. For instance, as mentioned in Section 3.3, the film roughness for the NO_2 condensate may also exist due to the potential inhomogeneity of NO_2 dimerization, which will be discussed in the following section.

4.3. Liquid Film Roughness Correction. Figure 9 shows the images of the liquid film taken at 2, 7, and 15 min during the condensation under a volume flow rate of 650 mL·min^{-1}, an air mole fraction of 70%, and a surface subcooling of 17 K. At different times in the condensation, the mixture of the film, droplets, and streamlets as marked in the figure can be constantly observed, directly leading to the liquid film roughness that differs from the traditional smooth film. On the basis of the above relationship between dimerization and HTC, it is reasonable to speculate that the inhomogeneity of NO_2 dimerization due to an uneven component concentration and temperature profiles in the condensation region is one of the reasons for uneven heat transfer distribution over the wall surface. The resultant heterogeneity of heat transfer contributes to varying existence of the condensate and thus the film roughness, which could be likely the reason for the values of experimental HTCs that are greatly underestimated by the theoretical model (Figure 7). On the one hand, the surfaces of droplets and streamlets exposed to the gas flow can increase the heat transfer area between the liquid film and the diffusion layer. On the other hand, with the condensate flowing downward, the

https://doi.org/10.1021/acsomega.2c00013
ACS Omega 2022, 7, 14735−14745

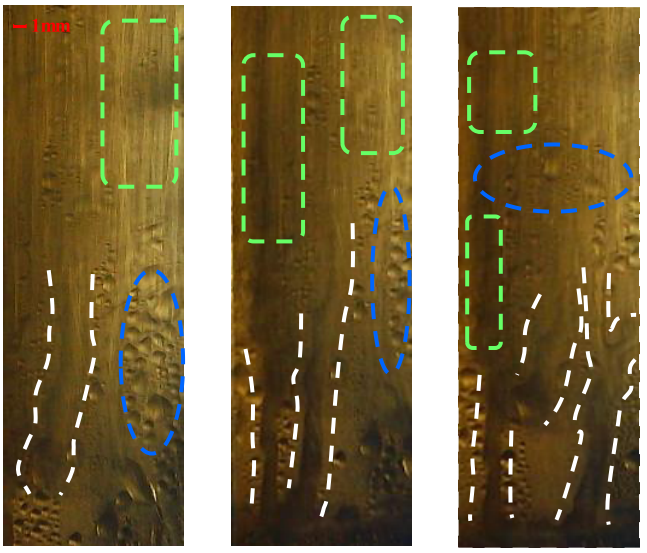

Figure 9. Condensate states (film, droplets, and streamlets marked by green, blue, and white dashed lines, respectively) visualized at different times during condensation.

surface morphology of the film changes constantly, causing disturbance to the gas diffusion layer.

To address the degradation factor for film roughness correction that follows $f_r = f(Re, w_{nc}, \Delta T)$ assumed in this work, the relationships of f_r with Re, ΔT, and w_{nc} can be established based on properties of the liquid film. Apparently, the roughness of liquid film depends on the proportion and distribution of the condensate film, streamlets, and droplets. Nevertheless, it is not easy to quantify the specific liquid amount and spatial distribution of each condensate state. The liquid amounts of the three condensate states constitute the total condensate amount that can be recorded in tests. Similarly to the film roughness, the flow rate of the total condensate ($q_{m,l}$, calculated via eq 8) varies with the status (proportion and distribution) of three condensates present at a specific moment. Therefore, there ought to be a certain correlation between liquid film roughness and $q_{m,l}$. Based on the experimental data at a NO_2−air mixture flow rate of 500 mL·min^{-1} and the relation of equations in Section 3.3, the curve of f_r versus $q_{m,l}$ can be depicted (Figure 10) and fitted with an equation showing a good correlation (R^2 = 0.81) as

$$f_r = 0.08 \times (1 + 0.1286 \times q_{m,l}^{-0.48}) \quad (32)$$

The value of $q_{m,l}$ representative of the macroscopic condensation efficacy varies with HTC that has close relationships with surface subcooling, Re, and NCG mole fraction, as shown in Sections 4.1 and 4.2. Therefore, the variation of $q_{m,l}$ with Re, ΔT, and w_{nc} as independent variables, can be fitted based on the experimental data at a NO_2−air mixture flow rate of 500 mL·min^{-1}, as listed in Table S3, rendering the correlation as

$$q_{m,l} = 0.0223 Re^{0.33} w_{nc}^{-0.49} \left(\frac{c_{p,NO_2}}{h_{fg,NO_2}} \Delta T\right)^{0.95} \quad (33)$$

Therefore, $q_{m,l}$ is introduced as a bridge between f_r and Re, ΔT, and w_{nc} to derive friction factor $f_r = f(Re, w_{nc}, \Delta T)$ based on eqs 32 and 33. Aiming to validate the accuracy of proposed f_r, eq 31 is replaced by eqs 32 and 33, and the product of f_c (eq 30) and

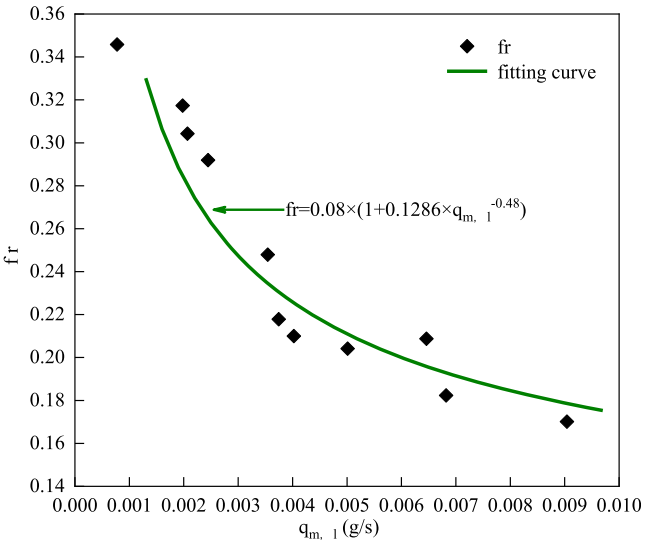

Figure 10. Experimental data and the fitting curve of f_r versus $q_{m,l}$.

HTC calculated from the modified model are compared with the experimental HTC. Note that the data used for verification, as shown in Table 2, and those for fitting eqs 32 and 33 (500 mL·min^{-1}) are independent. The verification results are shown in Figure 11: the horizontal axis represents the HTC calculated from the experimental data and the vertical axis represents the product of f_c and HTC calculated from the modified model. All of the calculated values fall within ±25% of the experimental

Table 2. Details of Experimental Data Used to Verify the Correlation between f_r and Re, ΔT, and w_{nc}

items	details
NCG	air
NCG mole fraction (%)	40, 50, 60, 70
inlet volume flow (mL·min^{-1})	250, 320, 650, 750
inlet Re number	60−360
surface subcooling (K)	8.4−20.5
pressure	0.1 MPa

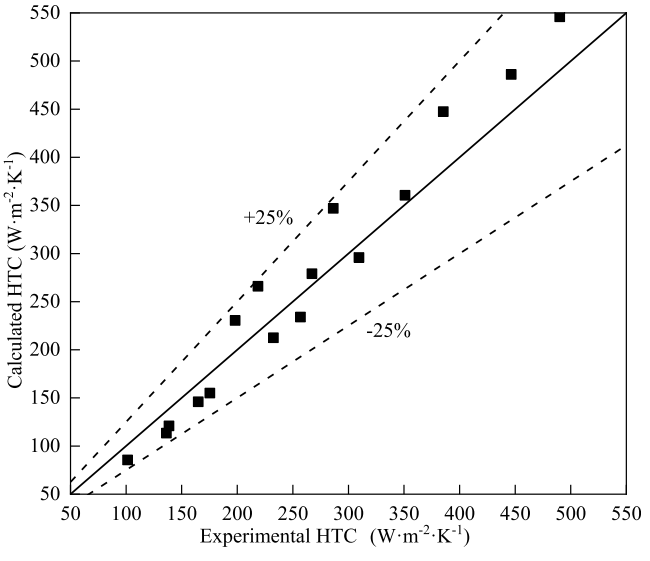

Figure 11. Comparison of calculated HTC with experimental HTC.

https://doi.org/10.1021/acsomega.2c00013
ACS Omega 2022, 7, 14735−14745

HTC, indicating the accuracy of the film roughness-corrected model prediction.

In eq 33, the exponent of each term reflects the effect of the corresponding variable on $q_{m,l}$, indicative of the condensation rate. Both *Re* and surface subcooling are positively correlated with $q_{m,l}$, while the NCG mole fraction is negatively correlated with $q_{m,l}$. The degree of the variable effect on $q_{m,l}$, indicated by the absolute value of the exponent, follows the order $\Delta T > w_{nc} > Re$ (0.95 > 0.49 > 0.3). Similarly, for film roughness correction that is described by the combination of eqs 32 and 33 and Section 3.3, the order of the degree of the variable effect follows $Re > \Delta T > w_{nc}$ (0.8 > 0.5 > 0.25). These results may indicate the mixed contributions from multiple factors to the NO_2 condensation heat transfer. The modified HMTA model in consideration of NO_2 dimerization and liquid film roughness correction would provide the key step for success in practical applications of NO_2 condensation.

5. CONCLUSIONS

In this paper, the condensation HTC of NO_2 was investigated using an experimental apparatus with a visualization system. The rough film of a NO_2 condensate with the coexistence of droplet, streamlet, and liquid film was observed. It was found that HTC increased with the decreases in surface subcooling and NCG mole fraction, and the increase in Re. There exist large discrepancies between experimental and classical HMTA model prediction results. The reasons lie in the effects of NO_2 dimerization on condensation, including the release of chemical reaction heat, the promotion of the mass transfer by increasing the NO_2 concentration gradient within the diffusion layer, and the liquid film roughness related to the heterogeneity of dimerization. A modified HMTA model considering changes in heat and mass transfer due to NO_2 dimerization was built. The effect of liquid film roughness on condensation was further corrected, improving the HTCs by 55 and 150%, respectively. In particular, the relationship between the liquid film roughness and each key parameter (inlet surface subcooling, NCG mole fraction, and Re) under NO_2 dimerization was addressed using the flow rate of the total condensate as an intermediary factor. Finally, an accurate prediction model for NO_2 condensation HTC in the presence of NCG within an error of ±25% was obtained, providing the key step for success in practical applications.

■ ASSOCIATED CONTENT

Supporting Information

The Supporting Information is available free of charge at https://pubs.acs.org/doi/10.1021/acsomega.2c00013.

Title page, saturated vapor pressures of N_2O_4 and NO_2 at corresponding temperatures, methodology for the calculation of the chemical heat flow rate from the initial state with pure NO_2 to the reaction equilibrium, methodology for liquid film heat transfer coefficient h_f calculation, methodology for latent heat transfer coefficient h_c calculation, molar fractions of N_2O_4 and NO_2 at different temperatures, and details of experimental data for multivariate nonlinear fitting of eq 33 (PDF)

■ AUTHOR INFORMATION

Corresponding Author

Ziyi Li − *School of Energy and Environmental Engineering, University of Science and Technology Beijing, Beijing 100083, China*; orcid.org/0000-0002-1947-9790; Phone: +86-01-62332743; Email: ziyili@ustb.edu.cn; Fax: +86-01-62334210

Authors

Yingshu Liu − *School of Energy and Environmental Engineering, University of Science and Technology Beijing, Beijing 100083, China*

Jiaxin Liu − *School of Energy and Environmental Engineering, University of Science and Technology Beijing, Beijing 100083, China*; orcid.org/0000-0001-5616-7609

Ningqi Sun − *School of Energy and Environmental Engineering, University of Science and Technology Beijing, Beijing 100083, China*

Xiong Yang − *School of Energy and Environmental Engineering, University of Science and Technology Beijing, Beijing 100083, China*

Huanyu Hou − *Group Strategy Research Institute, HBIS, Shijiazhuang 050023, China*

Wenhai Liu − *School of Energy and Environmental Engineering, University of Science and Technology Beijing, Beijing 100083, China*

Chunyu Zhao − *School of Energy and Environmental Engineering, University of Science and Technology Beijing, Beijing 100083, China*

Ralph T. Yang − *Department of Chemical Engineering, University of Michigan, Ann Arbor, Michigan 48109-2136, United States*; orcid.org/0000-0002-5367-9550

Complete contact information is available at: https://pubs.acs.org/10.1021/acsomega.2c00013

Notes

The authors declare no competing financial interest.

■ ACKNOWLEDGMENTS

The authors would like to express their gratitude to the National Natural Science Foundation of China (No. 21808012) and the Fundamental Research Funds for the Central Universities (Nos. FRFIDRY-19-025, QNXM20210028).

■ NOMENCLATURE

a	the channel half-width [m]
A	vertical wall area [m^2]
B_m,B_h	the suction parameter
Cp	specific heat [$J \cdot kg^{-1} \cdot K^{-1}$]
D	diffusion coefficient [$m^2 \cdot s^{-1}$]
f	friction factor
g	acceleration due to gravity [$m \cdot s^{-2}$]
h	heat transfer coefficient [$W \cdot m^{-2} \cdot K^{-1}$]
h_{fg}	heat of liquefaction [$J \cdot kg^{-1}$]
K_p	pressure equilibrium constant [Pa]
L	characteristic length [m]
m''	condensation mass flux [$kg \cdot m^{-2} \cdot s^{-1}$]
M	molar mass [$g \cdot mol^{-1}$]
P, p	total pressure [Pa]
Pr	Prandtl Number
$\dot{Q}$	heat flow rate [W]
q	heat flux [$W \cdot m^{-2}$]
q_m	mass flow rate [$g \cdot s^{-1}$]
Re	Reynolds number
Sc	Schmidt number
Sh	Sherwood number
t	time [s]

https://doi.org/10.1021/acsomega.2c00013
ACS Omega 2022, 7, 14735−14745

T	temperature [K]
V	volume [m^3]
w	mole fraction
w_m	mass fracton
x	vertical distance [m]
ρ	density [$kg \cdot m^{-3}$]
μ	dynamic viscosity [Pa·s]
λ	thermal conductivity [$W \cdot m^{-1} \cdot K^{-1}$]
δ	liquid film thickness [m]

SUBSCRIPTS

b	bulk
f	film
i	interface
l	liquid
w	wall
mix	gas mixture
r	reaction
in	inlet
out	outlet

REFERENCES

(1) Naimi-Jamal, M. R.; Hamzeali, H.; Mokhtari, J.; Boy, J.; Kaupp, G. Sustainable synthesis of aldehydes, ketones or acids from neat alcohols using nitrogen dioxide gas, and related reactions. *ChemSusChem* **2009**, *2*, 83−88.

(2) Liu, W. G.; Goddard, W. A., 3rd. First-principles study of the role of interconversion between NO_2, N_2O_4, cis-ONO-NO_2, and trans-ONO-NO_2 in chemical processes. *J. Am. Chem. Soc.* **2012**, *134*, 12970−12978.

(3) Tan, W.; Desheng, D. Discussion of Increase Product of Nitrogen Tetroxide. *Chem. Intermed.* **2007**, *05*, 28−30.

(4) Gan, L.; Xu, F.; Tian, B.; Wu, Y. In *Design of the Method of Condensing and Reclaiming N2O4 exhaust*,13th Natural Conference on Signal Intelligence informatics Processes Applied, Hanzhong, Shaanxi, China, 2019 ; p 5.

(5) Liu, Y.; You, Y.; Li, Z.; Yang, X.; Wu, X.; Zhao, C.; Xing, Y.; Yang, R. T. NOx removal with efficient recycling of NO_2 from iron-ore sintering flue gas: A novel cyclic adsorption process. *J. Hazard. Mater.* **2021**, *407*, No. 124380.

(6) Zhang, M.; Zhu, X.; Zhang, L.; Li, Y.; Li, J.; Xia, X.; Ma, C.; Dong, Y. Intensification of NOx Conversion over Activated Coke by Ozone Oxidation for Sintering Flue Gas at Low Temperatures. *ACS Omega* **2021**, *6*, 13484−13495.

(7) Zhang, L.; Hou, Z.; Huang, L.; Gu, P.; Xu, Z. In *Simulationand Practice of Condensation Recovery of Nitrogen Tetroxide Based on HYSYS*, In IOP Conference Series: Earth and Environmental Science, IOP Publishing, 2019; p 281.

(8) Liu, Y.; Sun, N.; Li, Z.; Xiao, P.; Xing, Y.; Yang, X.; Zhao, C.; Zhang, C.; Wang, H.; Yang, R. T.; et al. Recovery of high-purity NO_2 and SO_2 products from iron-ore sintering flue gas by distillation: process design, optimization and analysis. *Sep. Purif. Technol.* **2021**, *264*, No. 118308.

(9) Darani, N. S.; Behbahani, R. M.; Shahebrahimi, Y.; Asadi, A.; Mohammadi, A. H. Simulation and Optimization of the Acid Gas Absorption Process by an Aqueous Diethanolamine Solution in a Natural Gas Sweetening Unit. *ACS Omega* **2021**, *6*, 12072−12080.

(10) Egoshi, N.; Kawakami, H.; Asano, K. Heat and mass transfer model approach to optimum design of cryogenic air separation plant by packed columns with structured packing. *Sep. Purif. Technol.* **2002**, *29*, 141−151.

(11) Othmer, D. F. The condensation of steam. *Ind. Eng. Chem.* **1929**, *21*, 576−583.

(12) Al-Diwany, H.; Rose, J. Free convection film condensation of steam in the presence of non-condensing gases. *Int. J. Heat Mass Transfer* **1973**, *16*, 1359−1369.

(13) Gribkova, V. P.; Mikhalevich, A. A.; Nesterenko, V. B. Condensation of a chemically reacting gas on a vertical surface. *J. Eng. Phys.* **1972**, *22*, 699−704.

(14) Mikhalevich, A. A.; Fedosova, V. K. Condensation of a chemically reactive gas on a horizontal tube. *J. Eng. Phys.* **1981**, *40*, 478−483.

(15) Peterson, P.; Schrock, V.; Kageyama, T. Diffusion layer theory for turbulent vapor condensation with noncondensable gases. *J. Heat Transfer* **1993**, *115*, 998−1003.

(16) Xu, H.; Sun, Z.; Gu, H.; Li, H. Forced convection condensation in the presence of noncondensable gas in a horizontal tube; experimental and theoretical study. *Prog. Nucl. Energy* **2016**, *88*, 340−351.

(17) Park, S.; Kim, M.; Yoo, K. Effects of a wavy interface on steam-air condensation on a vertical surface. *Int. J. Multiphase Flow* **1997**, *23*, 1031−1042.

(18) Kang, H.; Kim, M. Effect of non-condensable gas and wavy interface on the condensation heat transfer in a nearly horizontal plate. *Nucl. Eng. Des.* **1994**, *149*, 313−321.

(19) Dehbi, A.; Guentay, S. A model for the performance of a vertical tube condenser in the presence of noncondensable gases. *Nucl. Eng. Des.* **1997**, *177*, 41−52.

(20) Ge, M.; Wang, S.; Zhao, J.; Zhao, Y.; Liu, L. Condensation of steam with high CO_2 concentration on a vertical plate. *Exp. Therm. Fluid Sci.* **2016**, *75*, 147−155.

(21) Lee, K. -Y.; Kim, M. H. Effect of an interfacial shear stress on steam condensation in the presence of a noncondensable gas in a vertical tube. *Int. J. Heat Mass Transfer* **2008**, *51*, 5333−5343.

(22) Kuhn, S.; Schrock, V.; Peterson, P. An investigation of condensation from steam−gas mixtures flowing downward inside a vertical tube. *Nucl. Eng. Des.* **1997**, *177*, 53−69.

(23) Ren, B.; Zhang, L.; Cao, J.; Xu, H.; Tao, Z. Experimental and theoretical investigation on condensation inside a horizontal tube with noncondensable gas. *Int. J. Heat Mass Transfer* **2015**, *82*, 588−603.

(24) Amoruso, A.; Crescentini, L.; Fiocco, G.; Volpe, M. New measurements of the NO_2 absorption cross section in the 440-to 460-nm region and estimates of the NO_2-N_2O_4 equilibrium constant. *J. Geophys. Res.* **1993**, *98*, 16857−16863.

(25) Chao, J.; Wilhoit, R. C.; Zwolinski, B. J. Gas phase chemical equilibrium in dinitrogen trioxide and dinitrogen tetroxide. *Thermochim. Acta* **1974**, *10*, 359−371.

(26) Haji-Sheikh, A.; Beck, J. V. Entrance effect on heat transfer to laminar flow through passages. *Int. J. Heat Mass Transfer* **2007**, *50*, 3340−3350.

(27) Kanatani, K. Reconsideration of correlation for condensation outside a vertical tube in the presence of noncondensable gas. *Int. J. Heat Mass Transfer* **2019**, *136*, 427−435.

(28) Ge, M.; Zhao, J.; Wang, S. Experimental investigation of steam condensation with high concentration CO_2 on a horizontal tube. *Appl. Therm. Eng.* **2013**, *61*, 334−343.

(29) Hu, H. W.; Tang, G. H.; Niu, D. Experimental investigation of condensation heat transfer on hybrid wettability finned tube with large amount of noncondensable gas. *Int. J. Heat Mass Transfer* **2015**, *85*, 513−523.

(30) Park, S.; Kim, M.; Yoo, K. Condensation of pure steam and steam-air mixture with surface waves of condensate film on a vertical wall. *Int. J. Multiphase Flow* **1996**, *22*, 893−908.

(31) Oh, S.; Revankar, S. T. Effect of noncondensable gas in a vertical tube condenser. *Nucl. Eng. Des.* **2005**, *235*, 1699−1712.

https://doi.org/10.1021/acsomega.2c00013
ACS Omega 2022, 7, 14735−14745